# INTERNAL GRAVITY WAVES IN A STABLY STRATIFIED BOUNDARY LAYER

ANNE F. DE BAAS and A. G. M. DRIEDONKS

*Institute for Meteorology and Oceanography, University of Utrecht, Netherlands*

*and*

*Royal Netherlands Meteorological Institute, De Bilt, Netherlands*

(Received in final form 17 August, 1984)

**Abstract.** Often, a combination of waves and turbulence is present in the stably stratified atmospheric boundary layer. The presence of waves manifest itself in the vertical profiles of variances of fluctuations and in low-frequency contributions to the power spectra. In this paper we study internal waves by means of a linear stability analysis of the mean profiles in a stably stratified boundary layer and compare the results with observed vertical variance profiles of fluctuating wind and temperature along a 200 m mast. The linear stability analysis shows that the observed mean flow is unstable for disturbances in a certain frequency and wavenumber domain. These disturbances are expected to the detectable in the measurements. It is shown that indeed the calculated unstable frequencies are present in the observed spectra. Furthermore, the shape of the measured vertical variance profiles, which increase with height, is explained well by the calculated vertical structure of the amplitude of unstable Kelvin–Helmholtz waves, confirming the contribution of waves to the variances. Because turbulence and waves have quite distinct transport properties, estimates of diffusion from measurements of variances would strongly overestimate this diffusion. Therefore it is important to distinguish between them.

## 1. Introduction

The vertical structure of the stably stratified boundary layer (SSBL) of the atmosphere, e.g., during a clear night over land, is dominated by radiational cooling of the surface. The resulting stable temperature gradient inhibits vertical exchange. Turbulence will be suppressed, except in a relatively thin ($\sim$ 100–200 m) layer near the ground where the vertical wind shear is large enough to overcome the effects of the stable stratification. Therefore one would expect the turbulent kinetic energy, in particular $\sigma_w^2$ (variance of vertical velocity fluctuations) and also $\sigma_\theta^2$ (variance of temperature fluctuations) to decrease as a function of height, and to be zero above the boundary layer.

Measurements show that in spite of a stable stratification the variances do not always decrease monotonically with height and even may increase. In Figures 1 and 2 an example is given of measurements of the vertical profiles of hourly mean quantities and variances in the nocturnal boundary layer along the 200 m mast at Cabauw, the Netherlands on the 30th of May, 01–02 UT. See Driedonks *et al.* (1978) for a description of the 200 m mast. The boundary-layer height (as inferred from acoustic sounder observations) was 180 m at the time. The increase of the variances with height is presumably caused by internal gravity waves, which can easily be generated in the stable atmosphere and which contribute to the variances. The traces of the temperature as a function of time given in Figure 3 for different heights demonstrate this phenomenon.

*Boundary Layer Meteorology* **31** (1985) 303–323. 0006–8314/85/0313–0303$03.15.

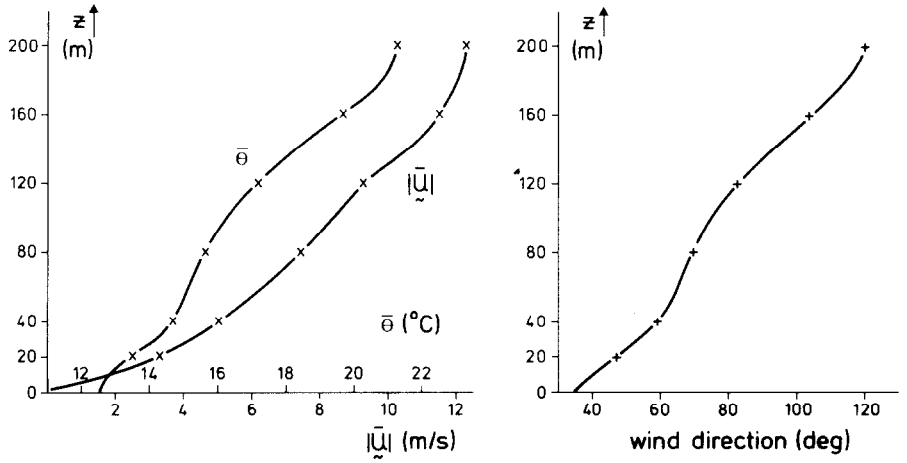


Fig. 1. (a) Measured vertical profiles of hourly mean wind speed ($\bar{u}$) and potential temperature ($\bar{\theta}$) at Cabauw, 30 May 1978, 01–02 UT. The height of the boundary layer was appr. 180 m. (b) Measured vertical profile of wind direction for the same period.

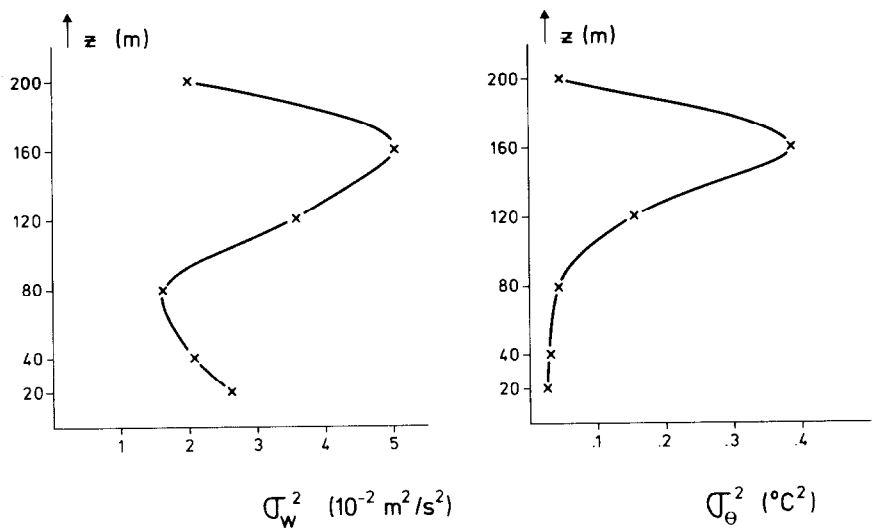


Fig. 2. Variance profiles of vertical wind fluctuations ($\sigma_w$) and potential temperature fluctuations ($\sigma_\theta$) measured on 30 May, 1978, 01–02 UT.

The structure of the SSBL is determined by a mixture of turbulence and waves. The dynamical properties of neutral waves and turbulence are quite different. Turbulence has the property of efficiently mixing pollutants while linear waves do not transport any pollutant at all. The discrimination between the two is of practical importance in diffusion models. Estimates of diffusion from measurements of variances would strongly overestimate the diffusion in these cases.

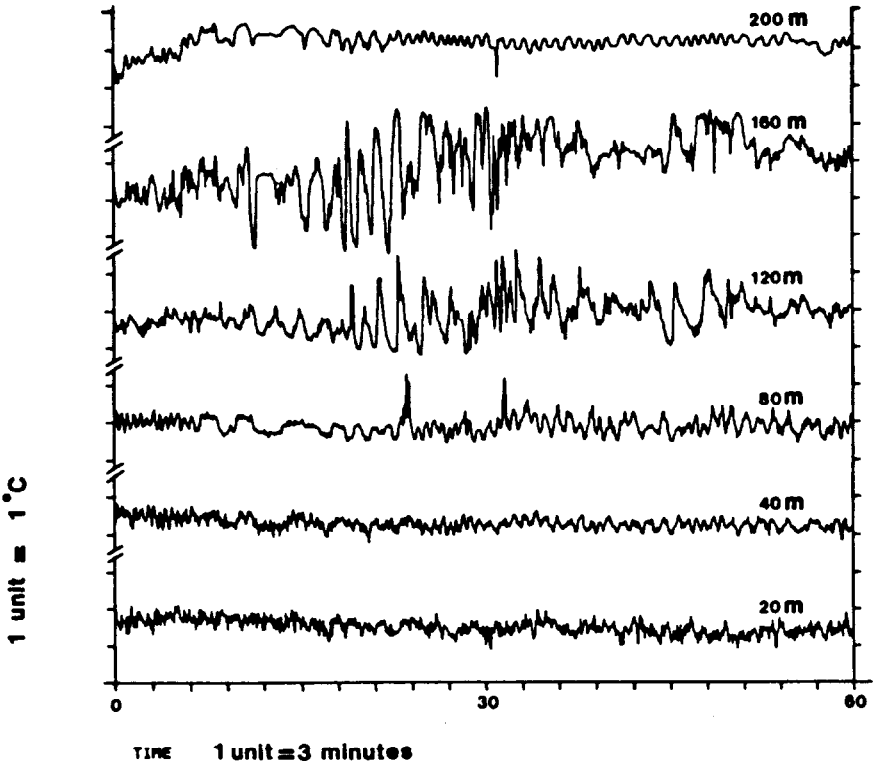


Fig. 3. Temperature traces at several heights as a function of time, 30 May, 1978, 01–02 UT. Temp. units in °C.

Various approaches have been made to differentiate theoretically and experimentally between waves and turbulence. Busch (1969) and Stewart (1969) have suggested criteria which would enable one to determine experimentally whether or not a given field of fluctuations is due to turbulence or to waves. This method is based on the different spectral properties of waves and turbulence. Caughey and Readings (1975), Caughey (1977), and Caughey *et al.* (1979) applied this spectral method to the SSBL. They came to the conclusion that if waves and turbulence have a comparable intensity, this spectral method works only if the waves and turbulence have different frequencies.

In this paper we look at the kind of waves that are supported by the background profiles of wind and temperature. It is well known (Drazin and Reid, 1981, p. 320) that there are at least two classes of wave-like solutions: neutrally stable waves that do not grow in time, and unstable waves that have an exponentially growing amplitude.

Neutrally stable waves are usually excited by some external influence on the flow, e.g., by topographical effects or by convective air bubbles that impinge on a stable layer capping a convective boundary layer. They also can enter the domain under consideration from outside. Fua *et al.* (1982) analysed the interaction between a neutrally stable monochromatic wave and a turbulent field. Einaudi and Finnigan (1981) and Finnigan

and Einaudi (1981) analysed a case with a monochromatic wave in a turbulent boundary layer, utilizing phase-averaging to discriminate between the wave and the turbulence.

The occurrence of unstable waves with an exponentially growing amplitude is most interesting since they can grow out of small disturbances of the background flow into waves with detectable amplitude, feeding on the mean wind shear. In this paper we shall especially investigate the background flow for these unstable perturbations.

Several other studies applied linear stability analysis to a background flow but not with observed profiles and not in comparison with measurements. Davis and Peltier (1976), Lalas and Einaudi (1976), and Fritts (1980) studied the excitation of gravity waves by shear flow instabilities of a hyperbolic tangent velocity profile bounded below by a rigid wall. Davis and Peltier assumed the temperature profile to be an hyperbolic tangent too, while the other studies assumed an exponential temperature profile. They all found a finite and predictable number of unstable modes, one of which is the well-known Kelvin–Helmholtz disturbance.

We performed a case study of measurements in the stably stratified nighttime boundary layer. The stability analysis is applied to the background profiles of wind and temperature, here taken as the time-averaged or mean state, and its solutions are compared with experimental spectra of fluctuating wind and temperature. The measurements were taken along the 200 m mast at Cabauw, the Netherlands (for a description see Driedonks *et al.* (1978)).

## 2. Theory

### 2.1. Model of the atmosphere

To study the excitation of gravity waves by shear flow instabilities, we consider a stratified shear flow in the SSBL, bounded below the ground and above by an infinite layer with a uniform wind and a constant temperature gradient.

We consider small perturbations on a background or mean state that is characterized by $p_0(z)$, $\rho_0(z)$, $\theta_0(z)$, and $\mathbf{v}_0 = (u_0(z), v_0(z), 0)$ in which $p$ is pressure, $\rho$ is density, $\theta$ is potential temperature and $\mathbf{v}$ is the wind vector. The index 0 denotes the background or reference state. The governing equations are the equation of conservation of mass, the momentum equations, the energy equation and the equation of state. The flow is assumed to be adiabatic and horizontally homogeneous. The effects of the rotation of the earth and of viscosity are assumed to be negligible.

We linearize the equations for small perturbations around the reference state, and apply the Boussinesq approximation and Squire's theorem (Betchov and Criminale, 1967, p. 101). Squire's theorem leads to the conclusion that solving the linear stability analysis for plane waves in a background wind field, that has shear in its magnitude as well as in its direction, is equivalent to solving it for the projection of the wind field on the wave-vector direction.

We consider perturbations $\alpha$ in the form of plane waves:

$$\alpha = \mathrm{Re}\{\hat{a}(z) \exp(i(kx - \sigma t))\} \tag{1}$$

with $k$ the wavenumber in the $x$-direction and $\sigma = \sigma_r + i\sigma_i$ the complex angular frequency. When $\sigma_i < 0$, the disturbance is stable; for $\sigma_i = 0$ neutral, and for $\sigma_i > 0$, the disturbance is unstable.

As the amplitude of unstable perturbations becomes larger, linear theory can not be used anymore. To investigate what happens to the disturbances then, non-linear interaction should be taken into account. We do not discuss that.

The linearized equations are (see e.g., Gossard and Hooke, 1975):

$$ik\hat{u} + \partial\hat{w}/\partial z = 0\,, \tag{2a}$$

$$\rho_0(-i\sigma + iku_0)\hat{u} + \rho_0\hat{w}\,\frac{\partial u_0}{\partial z} + ik\hat{p} = 0\,, \tag{2b}$$

$$\rho_0(-i\sigma + iku_0)\hat{w} + \frac{\partial\hat{p}}{\partial z} + g\hat{\rho} = 0\,, \tag{2c}$$

$$(-i\sigma + iku_0)\hat{\rho} - \frac{N^2\rho_0}{g}\,\hat{w} = 0\,. \tag{2d}$$

The Brunt-Väisälä frequency $N$ is given by

$$N^2 = -g\left(\frac{1}{\rho_0}\,\frac{\partial\rho_0}{\partial z} + \frac{g}{c_s^2}\right) \cong \frac{g}{\theta_0}\,\frac{\partial\theta_0}{\partial z}\,, \tag{3}$$

where $c_s$ is the speed of sound.

Since $u_0$ in (2) is the velocity component along the direction of **k**, we have to solve (1) and (2) for any direction $\phi$ of the wavenumber vector (the direction of the $x$-axis). However, since we are mainly looking for unstable solutions, the range of $\phi$ that is of interest is limited, as will be discussed in Section 3.1.

Elimination of $\hat{u}$, $\hat{p}$, and $\hat{\rho}$ in Equations (2a)–(2d) in favor of $\hat{w}$ leads, after some calculation, to the Taylor–Goldstein equation for $\hat{w}(z)$ (Gossard and Hooke, 1975, p. 123):

$$\frac{\mathrm{d}^2}{\mathrm{d}z^2}\,\hat{w}(z) + \Lambda(z)\hat{w}(z) = 0\,, \tag{4}$$

with

$$\Lambda(z) = \frac{N^2k^2}{\omega^2} - k^2 + \frac{k}{\omega}\,\frac{\mathrm{d}^2u_0}{\mathrm{d}z^2}\,, \tag{5}$$

and

$$\omega = \sigma - ku_0 = k(c - u_0)\,, \tag{6}$$

where $c$ is the phase speed

$$c = \sigma/k\,. \tag{7}$$

From Equation (2d) a useful relation between $\hat{\theta}$ and $\hat{w}$ follows:

$$\hat{\theta}(z) = -\frac{i}{\omega}\frac{N^2\theta_0}{g}\hat{w}(z)\,. \tag{8}$$

In order to solve Equation (4), we have to give boundary conditions. We take these as follows:

(i) at the ground,

$$z = 0 : \hat{w}(z) = 0\,, \tag{9}$$

(ii) above some height $z = z_u$, well above the boundary layer, $u_0(z)$ and $N^2(z)$ are taken constant. With a constant $\Lambda(z)$ in this region, the solution takes the form:

$$\hat{w}(z) \sim e^{inz}\,, \tag{10}$$

where $n$ is given by

$$n = (n_r + in_i) = \pm\{\Lambda(z)_u\}^{1/2} = \pm\left(\frac{N^2k^2}{(\sigma - u_0k)^2} - k^2\right)^{1/2}. \tag{11}$$

If $n_i \neq 0$, we take the solution with the exponentially damped amplitude, i.e., $n_i > 0$. If $n_i = 0$, and thus $n = n_r$, we require a radiation condition at $z = z_u$ with energy transport upward only. This means that we take the solution at $z = z_u$, which has an upward group velocity $c_{gz} = \partial\sigma/\partial n$. From Equation (11) it follows that we require

$$c_{gz} = \frac{\partial\sigma}{\partial n} = \frac{n(u_0k - \sigma)}{n^2 + k^2} > 0\,. \tag{12}$$

Thus, if $n_i = 0$, we take $n_r$ in Equation (11) to be the one that meets Equation (12). Thus $n_r > 0$ if $u_0k - \sigma > 0$ and $n_r < 0$ if $u_0k - \sigma < 0$. The Taylor Goldstein equation (4) and the boundary conditions (9)–(12) constitute a boundary-value problem. In Section 3 we will solve this and investigate the solutions.

If an unstable solution of this problem exists in the atmosphere, it will grow into a wave. Such a wave is detectable by our spectral method, to be discussed in Section 3.3.

## 2.2. Spectra

We analyse the measured wind and temperature spectra in terms of waves and turbulence.

The cross-spectrum $S_{w\theta}(k)$ is defined as the Fourier transform of the cross-correlation function $R_{w\theta}(r) = \overline{w(x)\,\theta(x + r)}$,

$$S_{w\theta}(k) = \int_{-\infty}^{\infty} R_{w\theta}(r)\,e^{+ikr}\,\mathrm{d}r = C_{w\theta}(k) - iQ_{w\theta}(k)\,, \tag{13}$$

where $C_{w\theta}(k)$ the co-spectrum and $Q_{w\theta}(k)$ the quadspectrum. We shall also use the

equivalent coherence $\mathrm{coh}_{w\theta}(k)$ and the phase-spectrum $\phi_{w\theta}(k)$, which are defined by:

$$\begin{aligned} \mathrm{coh}_{w\theta}(k) &= \| S_{w\theta}(k) \| / (S_w(k) \cdot S_\theta(k))^{1/2} , \\ S_{w\theta}(k) &= \| S_{w\theta}(k) \| \exp\{ -i\phi_{w\theta}(k) \} , \end{aligned} \tag{14}$$

where $S_w(k)$ and $S_\theta(k)$ denote the variance spectra (Bendat and Piersol, 1967, pp. 83–84); double bars denote absolute values of complex variables.

For disturbances in the form of Equation (1) we have

$$R_{w\theta}(r) = \frac{1}{4} e^{2\sigma_i t} \{ \hat{w}\hat{\theta}^* e^{-ikr} + \hat{w}^* \hat{\theta} e^{+ikr} \} , \tag{15}$$

where an asterisk denotes complex conjugate. Then

$$S_{w\theta}(k') = \frac{2\pi}{4} e^{2\sigma_i t} \{ \hat{w}\hat{\theta}^* \delta(k - k') + \hat{w}^* \hat{\theta} \delta(k + k') \} .$$

Through (8) we have

$$\hat{w}\hat{\theta}^* = \frac{-\sigma_i + i(\sigma_r - ku_0)}{(\sigma_r - ku_0)^2 + \sigma_i^2} \frac{N^2 \theta_0}{g} \| \hat{w} \|^2 , \tag{16}$$

and thus, for the one-sided spectral densities, the ratio of the cospectrum to the quadspectrum is:

$$\frac{C_{w\theta}}{Q_{w\theta}} = \frac{+\sigma_i}{\sigma_r - ku_0} . \tag{17}$$

Furthermore it follows that for our disturbances

$$\mathrm{coh}_{w\theta} = 1 , \tag{18}$$

$$\phi_{w\theta} = \arctan((\sigma_r - ku_0)/\sigma_i) . \tag{19}$$

For neutrally stable waves ($\sigma_i = 0$) we thus have

$$\begin{aligned} &C_{w\theta}/Q_{w\theta} = 0 \\ &\mathrm{coh}_{w\theta} = 1 \\ &\phi_{w\theta} = \pm \tfrac{1}{2}\pi . \end{aligned} \tag{20}$$

For unstable waves ($\sigma_i > 0$), usually $\sigma_i \ll \sigma_r$. Thus for those heights that are well away from the critical layer (where $\sigma_r = ku_0$), we may expect a spectral behavior as follows:

$$\begin{aligned} &C_{w\theta}/Q_{w\theta} \text{ small} \\ &\mathrm{coh}_{w\theta} = 1 \\ &\phi_{w\theta} \cong \tfrac{1}{2}\pi . \end{aligned} \tag{21}$$

When we are in the neighbourhood of a critical layer ($\sigma_r - ku_0$ small) the first and last condition of (21) will not necessarily apply. We then still may expect a large coherence.

The spectral properties of turbulence are quite different from Equations (20) or (21). Turbulence is a chaotic motion. The phase angles are randomly distributed between $-\pi$ and $+\pi$. Thus the criteria (20) or (21) give a method of discriminating between waves and turbulence in the spectra.

## 3. Method of Solution

In this section we will discuss the application of the stability analysis to measured wind and temperature profiles in a SSBL and the application of the spectral method to the fluctuation measurements of the same period.

The general restrictions on the solution of the Taylor–Goldstein equations will be discussed. In Section 3.3 the solution method of the Taylor–Goldstein equation is described as well as how the solutions appear in the spectra.

### 3.1. General restrictions on the solution

Solving the Taylor–Goldstein boundary value problem numerically without knowing the regions of the eigenvalues $(k, c)$ is endless work. However, without actually solving the problem we can already make restrictions on the solutions by using three criteria. We will discuss these in this section.

The first is a stability criterium based on the Richardson number; the second is the semi-circle theorem of Howard. The third is a restriction on the wave length.

A necessary condition for unstable wave solutions with a propagation direction $\phi$ is that the Richardson number Ri drops below 0.25 somewhere in the flow (Miles and Howard, 1964). The Richardson number is a measure of relative importance of the stabilizing influence of the stratification to destabilizing inertial effects and is defined by

$$\mathrm{Ri} = \frac{N^2}{(\partial u_0/\partial z)^2}\,, \tag{22}$$

where $u_0(z)$ is the profile of the wind components in the direction $\phi$. So if for a certain $\phi$ the value of Ri is larger than 0.25 everywhere, there are no unstable solutions in this direction. Therefore before starting to solve the Taylor–Goldstein equation for unstable modes, we first check if $\mathrm{Ri} < 0.25$ somewhere. When there is an inflection point in the wind profile (at $z = z_i$), then the minimum value of Ri in the profile will be found around this point, since the shear has a maximum there and $N^2$ varies in practice much more slowly with height than $(\partial u_0/\partial z)^2$.

The semi-circle theorem of Howard (Drazin and Reid, 1981, p. 142) limits the range of $c$-values for which unstable solutions possibly exist. According to this theorem a necessary condition for unstable solutions of the Taylor–Goldstein equation is that $c = (c_r, c_i)$ must lie within the semi-circle in the upper $c$-plane, whose diameter is

proportional to the greatest mean velocity difference $u_{max} - u_{min}$ in the layer considered, reduced by an amount depending on $N^2$:

$$[c_r - \tfrac{1}{2}(u_{min} + u_{max})]^2 + c_i^2 \leqq \tfrac{1}{4}(u_{min} - u_{max})^2 - \frac{\int_0^\infty N^2 \| \hat{w}^+ \|^2 dz}{\int_0^\infty P\, dz} \tag{23}$$

where $w^+ = w/(u_0 - c)$, and

$$P = \left\| \frac{\partial \hat{w}^+}{\partial z} \right\|^2 + k^2 \| \hat{w}^+ \|^2 > 0 .$$

This limits the $c$-values for which we apply the stability analysis.

The wavenumber $k$ of the unstable eigensolutions for a hyperbolic tangent profile has been calculated by e.g., Drazin (1958), Miles and Howard (1964) and Davis and Peltier (1976). They found that the wavelength $\lambda = 2\pi/k$ of the fastest growing instability ranges from 4 to 8 times the shear-layer depth, where the shear-layer depth is defined as the depth over which the gradient of the wind is large. In our calculations, we limited the range of $k$ that is searched for unstable solutions to 2 to 20 times the shear-layer depth as estimated from the measured profiles.

### 3.2. Description of the Numerical Stability Analysis

We have developed a computer program that determines unstable solutions of the Taylor–Goldstein equation (4) with the boundary conditions (9)–(12), for observed background vertical profiles of temperature, wind speed, and wind direction. This search has to be done in the domain of four parameters: $\phi$, the angle of the wave vector with the North–South direction (clockwise being positive); $k$, the length of the wave vector; $c_r$, the real part of the phase speed; and $c_i$, the complex part of the phase speed. We search for combination of these four parameters that give unstable solutions.

The angle $\phi$ was varied in small steps. For each value of $\phi$, the projection of the wind profile on this direction was calculated. This projected wind profile was investigated for meeting the Richardson-number criterion (Section 3.1) at some height. Only when this was the case, was the search continued for this $\phi$-value. Then the depth of the shear layer was estimated from the projected profile and the value of $k$ was varied in small steps between values corresponding to 2 to 20 times this depth.

For each value of $\phi$ and $k$, the upper semi-circle in the $(c_r, c_i)$-plane as given by (23) was searched for a possible unstable solution ($c_i \neq 0$). It is possible to do this with a shooting method, which iterates toward values of $(c_r, c_i)$ for which the boundary conditions are satisfied. A disadvantage of such a shooting method is that it can be sensitive to the values of the parameters $(c_r, c_i)$ chosen for starting the iteration. Another point is that only one solution is found, while there may be more.

To avoid these shortcomings, we developed a different solution method, which can be called a two-dimensional secant method. First the upper semi-circle in the $(c_r, c_i)$--plane was filled with a regular grid. For each of the grid points, the Taylor–Goldstein equation was integrated from $z = z_u$ down to $z = 0$ using a Merson integration technique (Lambert, 1973) giving $\hat{g}(z = 0) = \hat{w}_r(0) + i\hat{w}_i(0)$ for every grid point. We then look for the grid squares on whose four corners the calculated four values of both $\hat{w}_r(0)$ and $\hat{w}_i(0)$ change sign. For each of these grid squares, an iteration procedure is started. Three of the corners of such a grid square are used to define two planes: one through the three values of $\hat{w}_r(0)$, and one through the three values of $\hat{w}_i(0)$. These two planes intersect the horizontal plane of $\hat{w}_r(0) = \hat{w}_i(0) = 0$ along two lines. The intersection point (if any) of these two lines defines the new $(c_r, c_i)$ point, in the interation procedure. At this point again values of $\hat{w}_r(0)$ and $\hat{w}_i(0)$ are generated. Together with two out of the three values from the foregoing iteration step, they again define a new $(c_r, c_i)$-point by the intersection of planes. This iteration is continued until the new values found for $(c_r, c_i)$ do not differ more than a small amount from the old values. It must be remarked that for this method, as for the shooting method, no convergence is guaranteed. The iteration is stopped when the new values of $(c_r, c_i)$ are outside the semi-circle defined earlier. This whole iteration procedure was carried out for all relevant grid squares. Therefore this method can find more than one unstable solution, if present. However, in our case only one solution was found.

The search through the $(\phi, k, c_r, c_i)$-domain gives the possible sets of eigenvalues of these four parameters for which unstable solutions of the Taylor–Goldstein boundary-value problem exist. For each set of eigenvalues, the corresponding eigenfunctions $\hat{w}(z)$ and $\hat{\theta}(z)$ are calculated.

## 4. Results

### 4.1. Calculation of the unstable modes

First the unstable solutions of the Taylor–Goldstein boundary-value problem will be discussed and next the results of the spectral method.

We start with the input of the stability analysis, the measurements of the background flow. We chose a period of a stably stratified situation in which the variances of wind and temperature increased with height. The averaged wind and potential temperature profile measured on the 30th of May, 1978, 01–02 UT are shown in Figure 1 and tabulated in Table I. The temperature profile clearly shows the stable stratification of the boundary layer, which has a height of 180 m at the time (as inferred from acoustic sounder observations). The wind in this boundary layer turned more than 60° with height. Wind-shear vectors, calculated as the differences between winds at two heights, lie in the quadrant between North and West (Figure 4). The profiles of the velocity vectors were projected on a plane with direction $\phi$, where $\phi$ is the angle with the North–South direction, clockwise being positive, and $\phi$ is varied in steps of 20° (Figure 5, Table II).

TABLE I

Measured wind and temperature profiles

| $z$ | Windspeed | Wind direction | Potential temperature |
|---|---|---|---|
| 0 | 0 | 0 | 12.5 |
| 20 | 3.4 | 48 | 13.5 |
| 40 | 5.0 | 59 | 14.7 |
| 80 | 7.4 | 62 | 15.7 |
| 120 | 9.3 | 82 | 17.1 |
| 160 | 11.4 | 102 | 19.6 |
| 180 | 12.2 | 109 | 21.2 |

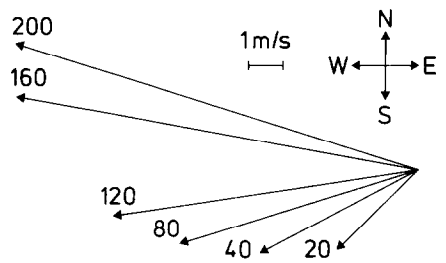


Fig. 4. Wind vectors at heights 20, 40, 80, 120, 160, and 200 m.

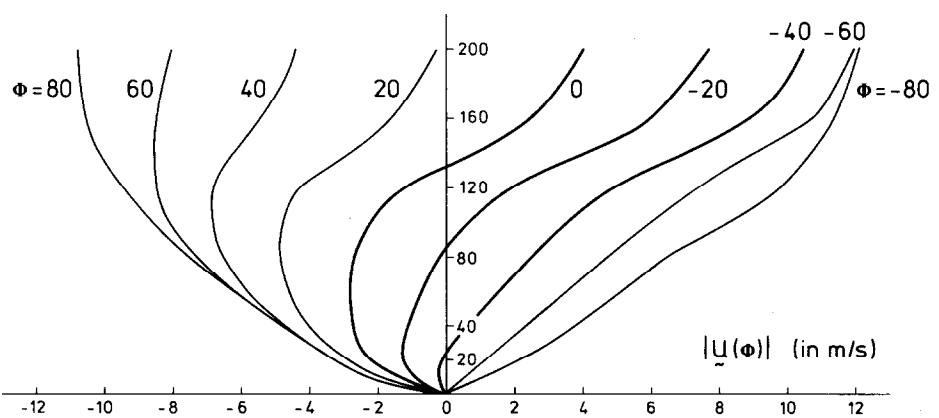


Fig. 5. Projected wind profiles on a vertical plane under an angle $\phi$ with the North–South direction.

The largest wind shear occurred in the profile of $\phi = -20°$ at the inflection point $z = 140$ m. The shear layer around this point has a depth of about 120 m.

The wind and temperature profiles being known, we search for the propagation directions in which the profiles meet the Ri < 0.25 criterion somewhere in the flow. For

TABLE II

Profiles of wind components in direction $\phi$

| $z$ \ $\phi$ | −80 | −60 | −40 | −20 | 0 | 20 | 40 | 60 | 80 |
|---|---|---|---|---|---|---|---|---|---|
| 0 | 0 | | 0 | 0 | 0 | 0 | 0 | 0 | 0 |
| 20 | 2.1 | 1.1 | −0.1 | −1.3 | −2.3 | −3.0 | −3.4 | −3.3 | −2.9 |
| 40 | 3.8 | 2.4 | 0.8 | −1.0 | −2.6 | −3.9 | −4.7 | −5.0 | −4.7 |
| 80 | 6.3 | 4.7 | 2.4 | −0.1 | −2.7 | −4.9 | −6.5 | −7.3 | −7.3 |
| 120 | 8.8 | 7.3 | 4.9 | 1.9 | −1.3 | −4.4 | −6.9 | −8.6 | −9.3 |
| 160 | 11.4 | 10.8 | 9.0 | 6.0 | 2.4 | −1.6 | −5.4 | −8.5 | −10.6 |
| 180 | 12.1 | 12.0 | 10.5 | 7.7 | 4.0 | −0.2 | −4.4 | −8.0 | −10.7 |

TABLE III

Richardson number profiles

| $z$ \ $\phi$ | −80 | −60 | −40 | −20 | 0 | 20 | 40 | 60 | 80 |
|---|---|---|---|---|---|---|---|---|---|
| 80 | 0.18 | 0.22 | 0.37 | 1.06 | 14.53 | 2.48 | 0.53 | 0.26 | 0.19 |
| 90 | 0.24 | 0.26 | 0.36 | 0.72 | 2.68 | 38.57 | 1.40 | 0.49 | 0.30 |
| 100 | 0.30 | 0.27 | 0.31 | 0.48 | 1.03 | 11.61 | 7.10 | 1.00 | 0.44 |
| 110 | 0.35 | 0.26 | 0.26 | 0.33 | 0.53 | 18.57 | 322.29 | 2.53 | 0.65 |
| 120 | 0.38 | 0.24 | 0.21 | 0.23 | 0.32 | 0.74 | 4.76 | 1.10 | 0.95 |
| 130 | 0.41 | 0.23 | 0.18 | 0.19 | 0.24 | 0.46 | 1.73 | 3.82 | 1.36 |
| 140 | 0.48 | 0.25 | 0.19 | 0.18 | 0.22 | 0.38 | 1.17 | 7.21 | 2.03 |
| 150 | 0.63 | 0.31 | 0.22 | 0.20 | 0.23 | 0.39 | 1.04 | 1.84 | 3.40 |
| 160 | 1.06 | 0.46 | 0.31 | 0.28 | 0.31 | 0.48 | 1.15 | 1.06 | 7.98 |
| 170 | 2.36 | 0.89 | 0.55 | 0.46 | 0.49 | 0.71 | 1.49 | 8.21 | 38.78 |
| 180 | 7.08 | 2.08 | 1.16 | 0.91 | 0.90 | 1.19 | 2.19 | 8.03 | 6566.60 |
| 190 | 34.67 | 6.53 | 3.13 | 2.22 | 2.05 | 2.45 | 3.97 | 10.73 | 192.36 |
| 200 | 97.26 | 2.92 | 12.21 | 8.03 | 7.05 | 7.91 | 11.78 | 27.13 | 207.50 |

every propagation direction $\phi$, the Richardson-number as a function of height is calculated around the inflection point (where Ri is smallest) (Table III).

From this table we see that the Richardson number criterion is only met by wind profiles projected on directions along the larger wind-shear vectors ($\phi = 0$ to $\phi = -40$). Therefore we only apply the stability analysis to this restricted interval of wave-propagation directions.

The wavenumber of the unstable waves is restricted by the shear-layer depth. The wind profiles from $\phi = 0°$ to $\phi = -40°$ all have a shear-layer depth of about 120 m around an inflection point at $z = 140$ m. We restricted the stability analysis to values of the wavenumber $k$ ranging from $2.5 \times 10^{-3}\,\mathrm{m}^{-1}$ to $25 \times 10^{-3}\,\mathrm{m}^{-1}$ (see Section 3.1).

The restrictions on $c$ from the semi-circle theorem depend on the range of wind speeds. This range is different for each $\phi$.

The stability analysis applied to these restricted combinations of $\phi$, $k$, and $c$ resulted in unstable eigensolutions that are shown in Table IV and Figure 6 where the angular frequency $\sigma_r$ is $c_r k$ and the growth rate $\sigma_i$ is $c_i k$.

TABLE IV

Solutions of the stability analysis for $\phi = -20$ and $\phi = -40$

| $k\,(10^{-3}\,\mathrm{m}^{-1})$ | $\sigma_r\,(10^{-2}\,\mathrm{Hz})$ | $\sigma_i\,(10^{-3}\,\mathrm{s}^{-1})$ |
|---|---|---|
| $\phi = 0$ | | |
| 7.5 | – | – |
| 10.0 | – | – |
| 12.5 | 1.2 | 1.1 |
| 15.0 | 1.4 | 2.7 |
| 17.5 | 1.7 | 2.4 |
| 20.0 | – | – |
| $\phi = -20$ | | |
| 5.0 | – | – |
| 7.5 | 2.0 | 1.6 |
| 10.0 | 3.2 | 5.1 |
| 12.5 | 4.3 | 6.3 |
| 15.0 | 5.4 | 5.9 |
| 17.5 | 6.5 | 4.0 |
| 20.0 | – | – |
| $\phi = -40$ | | |
| 5.0 | – | – |
| 7.5 | 3.7 | 2.3 |
| 10.0 | 4.4 | 3.7 |
| 12.5 | 7.4 | 5.0 |
| 15.0 | 9.2 | 3.9 |
| 17.5 | 11.1 | 1.3 |
| 20.0 | – | – |

From these results we conclude that unstable perturbations have wavenumbers within roughly the same range for each propagation direction ($k = 7.5 \times 10^{-3}\,\mathrm{m}^{-1} - 17.5 \times 10^{-3}\,\mathrm{m}^{-1}$). This was expected, because the shear-layer depth $h$ is roughly the same ($h \sim 120$ m) for this range of directions. The frequencies $\sigma_r = kc_r$ and growth rates $\sigma_i = kc_i$ of these unstable perturbations do vary with propagation direction. The real part of the phase velocity, $c_r$, is equal to the windspeed at the inflection point. The variation of the growth rate $\sigma_i$ resembles a parabola, with a maximum for wavelength $\lambda$ of 3 or 4 times the shear-layer depth.

As mentioned previously, the largest wind shear occurred in the direction $\phi = -20°$. The fastest growing wave calculated for this direction ($k = 1.5 \times 10^{-3}\,\mathrm{m}^{-1}$, $\sigma_r = 4 \times 10^{-2}$ Hz, $\sigma_i = 6 \times 10^{-3}\,\mathrm{s}^{-1}$) has indeed the largest growth rate of all possible unstable solutions.

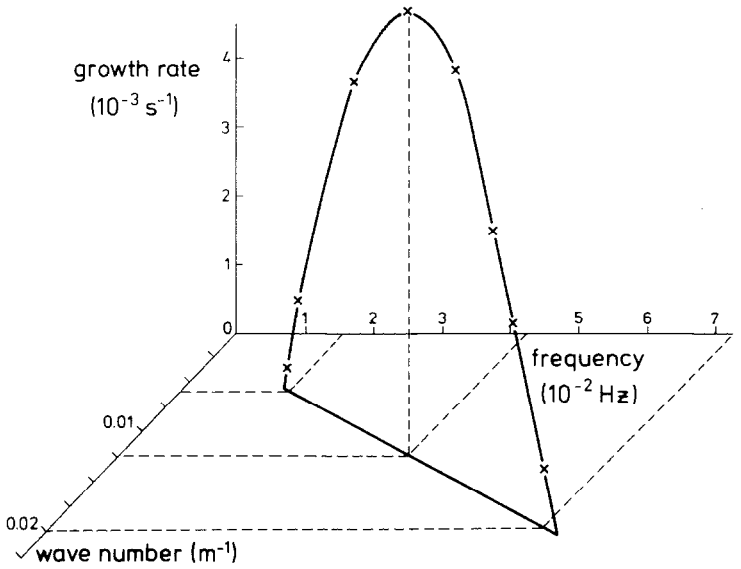


Fig. 6. Solution of the stability analysis for $\phi = -20$ where $k$ is wavenumber, $\sigma_r$ is angular frequency and $\sigma_i$ is growth-rate.

TABLE V

Squared amplitude of the vertical fluctuation velocity $\|\hat{w}\|^2$ and of the temperature fluctuation $\|\hat{\theta}\|^2$ of the solution with maximum growth rate normalised with the maximum value

| $z$ (m) | $\phi = 0$ | | $\phi = -20$ | | $\phi = -40$ | |
|---|---|---|---|---|---|---|
| | $\|\hat{w}\|^2$ | $\|\hat{\theta}\|^2$ | $\|\hat{w}\|^2$ | $\|\hat{\theta}\|^2$ | $\|\hat{w}\|^2$ | $\|\hat{\theta}\|^2$ |
| 0 | 0.00 | 0.00 | 0.00 | 0.00 | 0.00 | 0.00 |
| 20 | 0.14 | 0.02 | 0.04 | 0.00 | 0.01 | 0.00 |
| 40 | 0.28 | 0.03 | 0.11 | 0.01 | 0.05 | 0.00 |
| 60 | 0.45 | 0.04 | 0.22 | 0.01 | 0.12 | 0.00 |
| 80 | 0.72 | 0.05 | 0.40 | 0.03 | 0.24 | 0.00 |
| 100 | 0.98 | 0.07 | 0.57 | 0.07 | 0.38 | 0.01 |
| 120 | 0.86 | 0.10 | 0.50 | 0.23 | 0.35 | 0.02 |
| 130 | 0.52 | 0.14 | 0.29 | 1.00 | 0.26 | 1.00 |
| 140 | 0.12 | 1.00 | 0.32 | 0.12 | 0.45 | 0.01 |
| 160 | 0.82 | 0.12 | 0.88 | 0.00 | 0.94 | 0.01 |
| 170 | 1.00 | 0.10 | 1.00 | 0.00 | 1.00 | 0.01 |
| 180 | 0.99 | 0.08 | 0.99 | 0.00 | 0.95 | 0.01 |
| 200 | 0.76 | 0.06 | 0.78 | 0.00 | 0.72 | 0.01 |
| 220 | 0.48 | 0.05 | 0.53 | 0.00 | 0.48 | 0.01 |
| 240 | 0.28 | 0.04 | 0.33 | 0.00 | 0.30 | 0.01 |
| 260 | 0.17 | 0.03 | 0.22 | 0.00 | 0.19 | 0.01 |
| 280 | 0.10 | 0.03 | 0.14 | 0.00 | 0.13 | 0.01 |
| 300 | 0.06 | 0.02 | 0.09 | 0.00 | 0.08 | 0.01 |

For each $\phi$, the profile of the amplitude of the vertical fluctuation velocity $\hat{w}(z)$ of the fastest growing wave is calculated as well as the amplitude profile of the temperature fluctuation $\hat{\theta}(z)$. The energy contents $\|\hat{w}(z)\|^2$ and $\|\hat{\theta}(z)\|^2$ normalised with their maximum value are shown in Table V. The vertical velocity profiles have a typical Kelvin–Helmholtz structure: a minimum at the inflection point of the wind profile and two maxima at both sides. Only the shape of eigenfunctions is determined. The absolute value of the amplitudes of the eigenfunctions can not be determined as we used a eigenvalue problem to describe wave generation.

If we combine the results of the stability analysis for different propagation directions, we come to the conclusion that perturbations with a frequency $f = \sigma_r/2\pi$ from $3 \times 10^{-3}$ to $2 \times 10^{-2}$ Hz are unstable. Whenever these perturbations occur in the atmosphere, they will grow into waves and should become detectable by our spectral method.

### 4.2. Spectral analysis of the observations

The results of this spectral analysis will now be discussed. From the measured fluctuations of the vertical velocity $w'$ and of the (potential) temperature $\theta'$, the energy and cross-spectra are calculated. The energy spectra of $w'$ and $\theta'$ in Figure 7 show a large peak around $f = 10^{-2}$ Hz at heights 120, 160, and 200 m. This peak is investigated for linear wave properties.

The phase and coherence spectra of the heights 200 and 160 m (Figure 8) clearly show the properties of internal waves around this frequency: a very nearly constant phase of $\frac{1}{2}\pi$ and a large coherence (see Equations (20) and (21)). Outside this frequency interval, they are randomly distributed, which indicates turbulence.

The cospectrum and the quadspectrum of these heights, too, confirm the wave properties around $f = 10^{-2}$ Hz: the cospectrum is small and the quadspectrum large. The properties of the waves at a height 120 m were less clear.

The peak in the spectra around $f = 10^{-2}$ Hz has the same frequencies as the solutions of the stability analysis. Figures 7 and 8 show the solutions of the stability analysis depicted in the spectra. We draw the conclusion that all possible Kelvin–Helmholtz solutions were indeed excited in the atmosphere. This is in agreement with the conclusions of Davis and Peltier (1976), who state that the Richardson-number criterion is not only a necessary but also a sufficient condition for K.H. instabilities. Other waves, the so-called resonant waves, have growth rates that are much smaller than those of Kelvin–Helmholtz waves, if the latter are present.

### 4.3. Variance profiles

We also calculated the energy of the measured fluctuations in the frequency range from $3 \times 10^{-3}$–$2 \times 10^{-2}$ Hz. Figures 9 and 10 show these measured variances as well as the energy of the fastest growing K.H. waves for $\phi = -20$, both normalized with their maximum value.

Comparing the two vertical velocity variance profiles (Figure 9), we see that both show a maximum around $z = 170$ m. The second, smaller maximum of the calculated profile does not appear in the measurements. This is probably due to the fact that

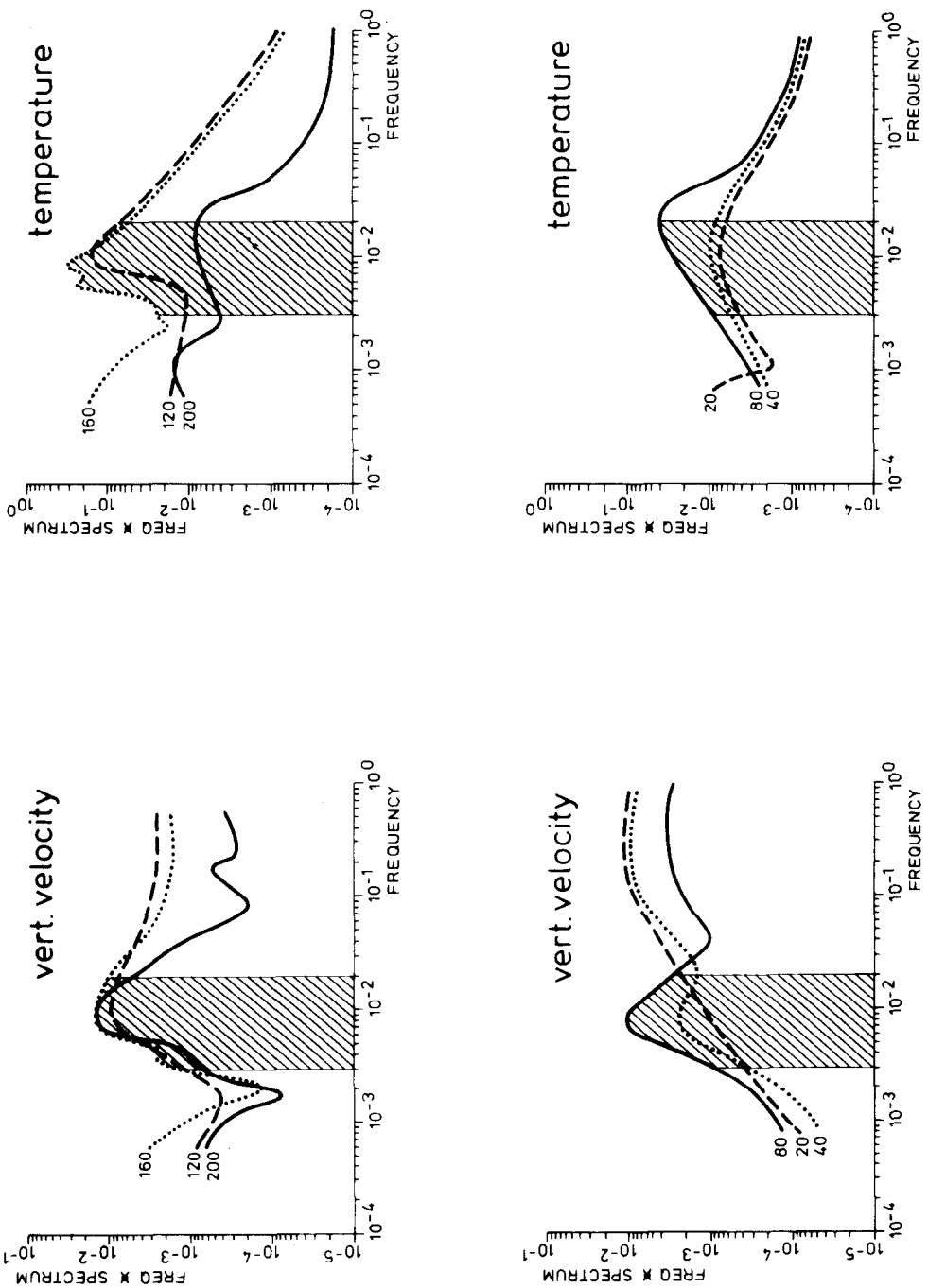


Fig. 7. Variance spectra of vertical velocity and temperature at 200, 160, 120, 80, 40, and 20 m height, 30 May, 1978, 01–02 UT. The striped area indicates all possible solutions of the stability analysis.

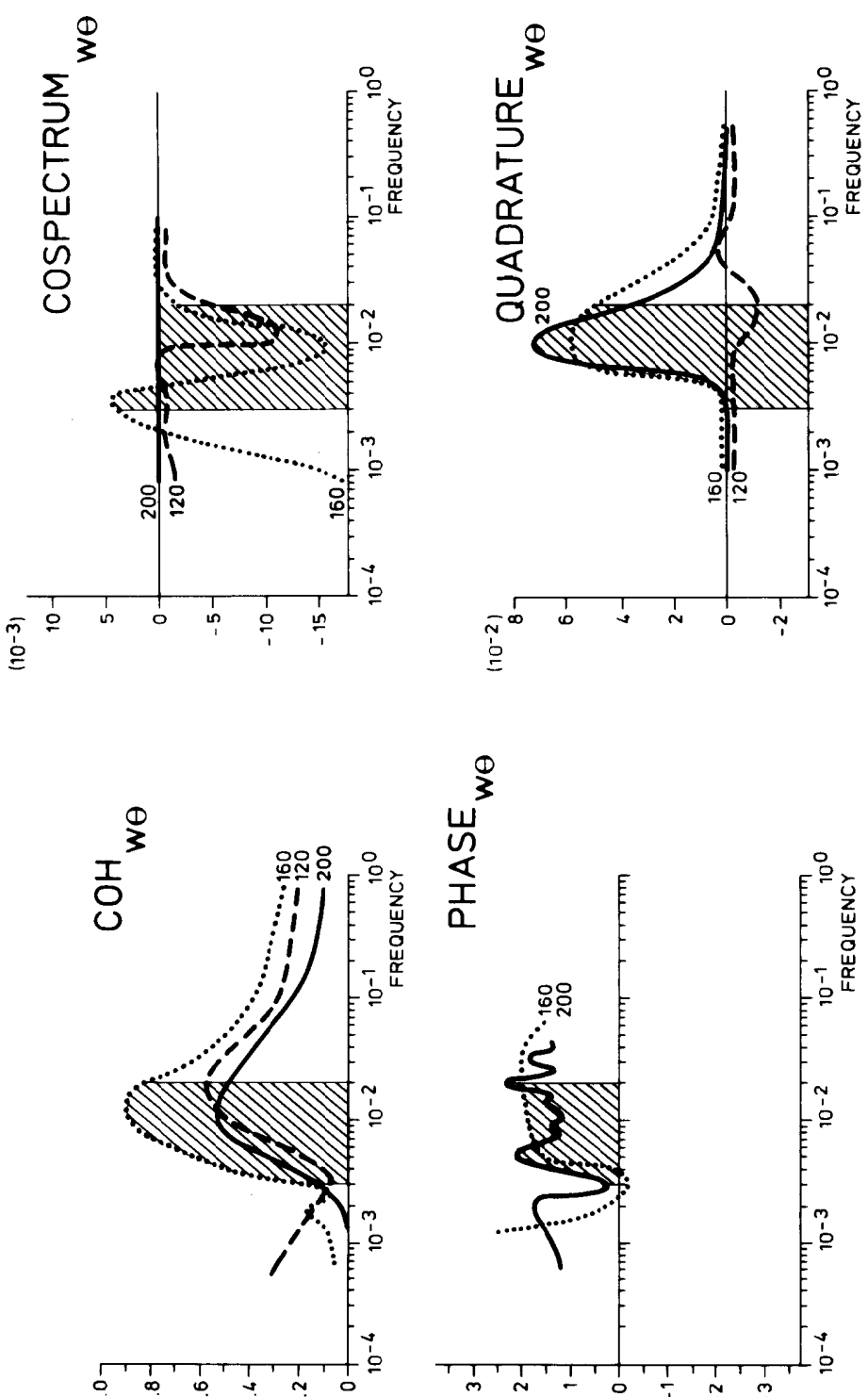


Fig. 8. Coherence, phase, co- and quadrature spectra of vertical velocity and temperature at 200, 160, 120 m height, 30 May, 11978, 01–02 UT. The phase spectra of 120 m is very irregular and therefore not plotted.

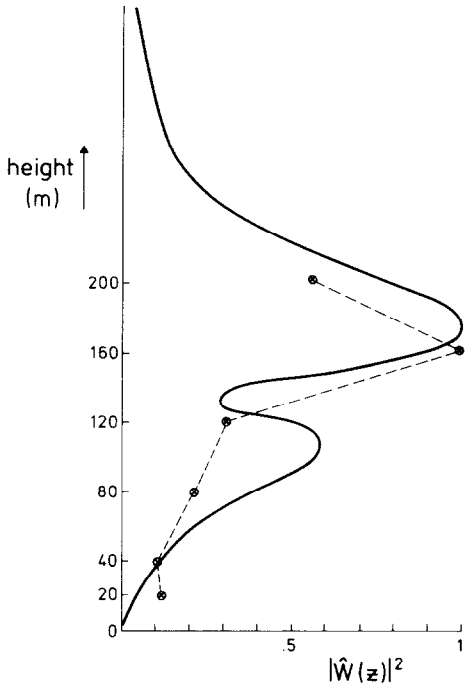


Fig. 9. Amplitude profile of the normalised vertical velocity fluctuations of the fastest growing solution for $\phi = -20$ and the measured vertical velocity fluctuations.

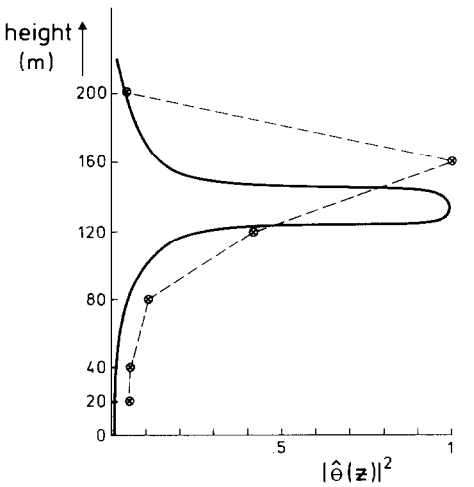


Fig. 10. Amplitude profile of the normalised temperature fluctuations of the fastest growing solution for $\phi = -20$ and the normalised measured temperature fluctuations.

turbulence is present in the atmosphere up to the boundary-layer height ($z$ = 180 m). This turbulence having its largest intensity at lower heights suppresses the wave structure there.

Figure 10 displays the measured and calculated temperature variance profiles for $\phi = -20$, both showing a large peak, the measured peak at a slightly greater height than the K.H. peak. We see that the structure of the K.H. waves is a good explanation for the observed anomalous variance profiles.

## 5. Discussion

In spite of the fact that we restricted our research to unstable waves generated by shear, while many more types of waves can be generated in a stably stratified atmosphere, we are able, in this case, to explain the 'wave part' of the spectra as being Kelvin–Helmholtz waves. The frequency interval $3 \times 10^{-3}$ Hz $< f < 2 \times 10^{-2}$ Hz showed wave properties and coincides with that of the unstable solutions of the linear stability analysis.

To be able to determine the contribution of waves to the measured fluctuations, we have to know the energy of the waves. But as stated before, from an eigen-value problem point of view, the frequencies and wavelengths can be determined but not the absolute value of the K.H. amplitudes. Nevertheless the calculated vertical structure of K.H. waves is an explanation for the measured variance profiles of the vertical velocity fluctuations and of the temperature fluctuations. The spectral method is only efficient in cases in which K.H. waves dominate over turbulence. Anomalies in the variance profiles due to waves occur in a stably stratified boundary layer where the turbulence is suppressed. Therefore the method we developed is sufficient to explain these anomalies.

It is not yet clear why the Kelvin–Helmholtz disturbances are indeed observed as waves during a period as long as an hour while the calculated typical time constant for growth is of order of 3 min. In this analysis, the non-linear effects are not taken into account. These forces however, might reduce the growth rate of the waves. Therefore the instabilities can be stabilized at a certain amplitude instead of breaking into turbulence. The frequencies which will be observed depend on the initial growth rate as well as on the non-linear effects (Lalas and Einaudi, 1976).

## 6. Summary and Conclusions

The aim of this research was to distinguish waves from turbulence and to explain measured anomalies in the stably stratified boundary layer, especially in the variance profiles of vertical velocity and potential temperature.

From turbulence theory, the variances of the vertical velocity and temperature in a stably stratified boundary layer are expected to decrease with height. Waves cause anomalous behavior of these variances. We restricted ourselves to shear-generated Kelvin–Helmholtz waves, which can be calculated with a linear stability analysis of the

Taylor–Goldstein boundary-value problem. The stability analysis has been applied to one hour of measurements on 30 May, 1978, 01–02 UT.

K.H. waves only feel the wind shear in their propagation direction. Therefore the analysis has been applied to profiles of wind components in propagation directions that met the Richardson number criterium for instabilities. The solutions form a continuous frequency interval of growing waves bounded by two neutrally stable solutions. The real phase velocity is equal to the wind velocity at the inflection point. The growth rate is a parabolic-like function of the wavenumber. The fastest growing solutions have a wavelength that is about 4 times the shear-layer depth.

These results for realistic profiles are in accordance with the results of Davis and Peltier (1976) who defined the frequencies, wavelengths, and growth rates of unstable disturbances of a hyperbolic tangent profile as functions of the parameters of the background flow.

Applying the spectral method to the fluctuation measurements, we see that the frequencies of the K.H. instabilities agree with an interval in the spectra that shows wave properties.

The form of the solutions $\hat{w}(z)$ and $\hat{\theta}(z)$ of the Taylor–Goldstein boundary value problem are an explanation for the measured variance profiles.

We can draw the conclusion that if we solve the Taylor–Goldstein equation for measured wind and temperature profiles, we find K.H. waves that can be found in the spectra. These waves explain the anomalous behaviour of the variance profiles in cases in which K.H. waves dominate over turbulence and other kinds of waves.

## Acknowledgements

Helpful discussions with Drs. F. T. M. Nieuwstadt, M. A. Weissman and P. A. E. M. Janssen as well as comments on earlier versions of the manuscript by Drs. A. C. M. Beljaars and H. Tennekes are gratefully acknowledged.

## References

Bendat, J. S. and Piersol, A. G.: 1966, *Measurements and Analysis of Random Data*, Wiley and Sons, New York.

Betchov, R. and Criminale, W. O.: 1967, 'Stability of Parallel Flows', *Applied Math. and Mech. Ser.* **10**, Acad. Press.

Busch, N. E.: 1969, 'Waves and Turbulence', *Radio Science* **4**, 1377–1379.

Caughey, S. J.: 1977, 'Boundary-Layer Turbulence Spectra in Stable Conditions', *Boundary-Layer Meteorol.* **11**, 3–14.

Caughey, S. J. and Readings, C. J.: 1975, 'An Observation of Waves and Turbulence in the Earth's Boundary Layer', *Boundary-Layer Meteorol.* **9**, 279–296.

Caughey, S. J., Wyngaard, J. C., and Kaimal, J. C.: 1979, 'Turbulence in the Evolving Stable Boundary Layer', *J. Atmos. Sci.* **6**, 1041–1052.

Davis, P. A. and Peltier, W. R.: 1976, 'Resonant Parallel Shear Instability in the Stably Stratified Planetary Boundary Layer', *J. Atmos. Sci.* **33**, 1287–1300.

Drazin, P. G.: 1958, 'The Stability of a Shear Layer in an Unbounded Heterogeneous Inviscid Fluid', *J. Fluid Mech.* **4**, 214–224.

Fritts, D. C.: 1980, 'Simple Stability Limits for Vertically Propagating Unstable Modes in a tanh($z$) Velocity Profile with a Rigid Lower Boundary', *J. Atmos. Sci.* **37**, 1642–1648.

Fua, D., Chimonas, G., Einaudi, F., and Zeman, O.: 1982, 'An Analysis of Wave-Turbulence Interaction', *J. Atmos. Sci.* **39**, 2450–2463.

Gossard, E. E. and Hooke, W. H.: 1975, *Waves in the Atmosphere; Atm. Infrasound and Gravity Waves Their Generation and Propagation*, Devel. in *Atm. Sci.* **2**, Amsterdam.

Lalas, D. P. and Einaudi, F.: 1976, 'On the Characteristics of Gravity Waves Generated by Atm. Shear Layers', *J. Atmos. Sci.* **13**, 1248–1259.

Lambert, J. D.: 1973, *Computational Methods in Ordinary Differential Equations*, Wiley and Sons, New York.

Miles, J. W. and Howard, L. N.: 1964, 'Note on a Heterogeneous Shear Flow', *J. Fluid Mech.* **20**, 331–336.

Stewart, R. W.: 1969, 'Turbulence and Waves in a Stratified Atmosphere', *Radio Science* **4**, 1269–1278.